LANGMUIR

pubs.acs.org/Langmuir Article

Characterizing the Locus of a Peripheral Membrane Protein−Lipid Bilayer Interaction Underlying Protein Export Activity in *E. coli*

Tina R. Matin,[$] Milica Utjesanovic,[$] Krishna P. Sigdel, Virginia F. Smith, Ioan Kosztin,* and Gavin M. King*

Cite This: *Langmuir* 2020, 36, 2143−2152 Read Online

ACCESS | Metrics & More | Article Recommendations

ABSTRACT: Quantitative characterization of the strength of peripheral membrane protein−lipid bilayer interactions is fundamental in the understanding of many protein targeting pathways. SecA is a peripheral membrane protein that plays a central role in translocating precursor proteins across the inner membrane of *E. coli*. The membrane binding activity of the extreme N-terminus of SecA is critical for translocase function. Yet, the mechanical strength of the interaction and the kinetic pathways that this segment of SecA experiences when in proximity of an *E. coli* polar lipid bilayer has not been characterized. We directly measured the N-terminal SecA-lipid bilayer interaction using precision single molecule atomic force microscope (AFM)-based dynamic force spectroscopy. To provide conformational data inaccessible to AFM, we also performed all-atom molecular dynamics simulations and circular dichroism measurements. The N-terminal 10 amino acids of SecA have little secondary structure when bound to zwitterionic lipid head groups, but secondary structure, which rigidifies the lipid-bound protein segment, emerges when negatively charged lipids are present. Analysis of the single molecule protein−lipid dissociation data converged to a well-defined lipid-bound-state lifetime in the absence of force, τ_0^{lipid} = 0.9 s, which is well separated from and longer than the fundamental time scale of the secretion process, defined as the time required to translocate a single amino acid residue (~50 ms). This value of τ_0^{lipid} is likely to represent a lower limit of the *in vivo* membrane-bound lifetime due to factors including the minimal system employed here.

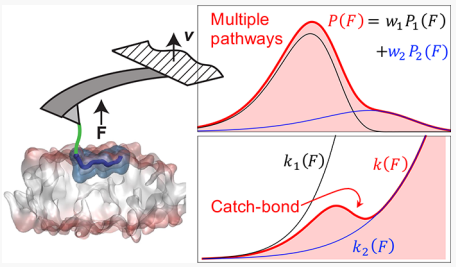

INTRODUCTION

Peripheral membrane proteins play a vital role in cell activity. To perform their functions, they need to properly bind to the cell membrane and do so at the correct time. The determination of where and the quantitative characterization of how this binding occurs are crucial, as this information can provide mechanistic insight into the function of these proteins. For example, the general secretory (Sec) system is the major route of export for proteins from the cytosol of *E. coli* and has homologues across all life forms. The peripheral membrane protein ATPase SecA is a central component of the Sec system. SecA binds integral membrane SecYEG (the translocon), forming the Sec translocase.[1,2] Though the field has advanced significantly from the acquisition of high resolution structural data, many questions remain regarding dynamic mechanisms underlying the complex process of secretion.

It has long been known that SecA binds acidic lipid to execute its function[3] and is not just associated with the translocon via protein−protein interactions (Figure 1a).[4−8] What region of SecA is involved with lipid binding? An elegant study from the Rapoport laboratory constructed a variant of SecA with the N-terminal segment deleted and replaced with a 6-His tag and a short linker.[9] This SecA mutant did not support translocation in standard proteoliposomes. However, when proteoliposomes were made with 10% Ni-NTA lipids—allowing a direct tether between SecA and the lipid bilayer surface—translocation of precursor protein was restored. Taken together with other work that demonstrates allosteric changes,[10] it is evident that SecA-lipid interactions are fundamental to the activity of the Sec system and that the extreme N-terminal region of this large protein (901 amino acids, monomer molecular weight 102 kDa) is involved with critical lipid interactions that enable translocase function.[11] Despite its key role in protein export function, the strength and kinetic pathway(s) governing *E. coli* lipid-SecA interactions have not been characterized.

Atomic force microscopy (AFM)-based single molecule force spectroscopy has been used to study the folding kinetics and structural energetics of individual membrane proteins. Most studies, however, have focused on unfolding large multimeric membrane proteins, such as bacteriorhodopsin, which are embedded in tightly packed arrays that suppress

Received: November 21, 2019
Revised: January 31, 2020
Published: February 3, 2020

https://dx.doi.org/10.1021/acs.langmuir.9b03606
Langmuir 2020, 36, 2143−2152

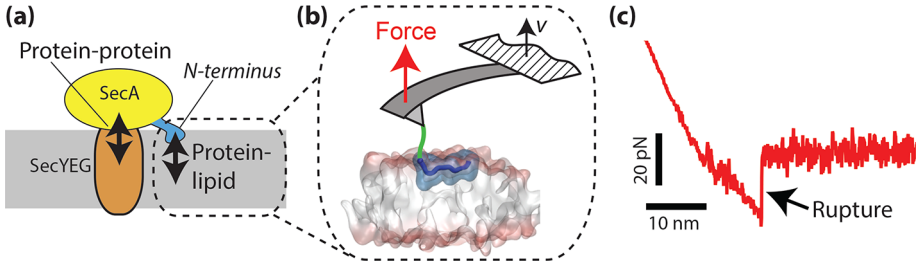

Figure 1. (a) Sketch showing two interactions that are likely to stabilize the translocase SecYEG/SecA at the cytoplasmic membrane interface of *E. coli*. This work is focused on the protein−lipid interaction emanating from the lipophilic N-terminus of SecA, blue. The remainder of SecA is drawn in yellow; SecYEG is drawn in orange. (b) Overview of the experiment. The AFM cantilever base, translated vertically at speed v, dissociates the N-terminal region of SecA from the bilayer. The linker is drawn in green, not to scale. (c) Force versus vertical position data for SecA2−11 and *E. coli* polar lipid. The arrow indicates a rupture (dissociation) event.

diffusion of both lipid and protein.[12,13] Directly probing protein interactions with supported lipid bilayers which maintain significant fluidity[14] comes with both experimental and theoretical challenges.[15−21] Previously, our group employed AFM-based force spectroscopy to probe the interaction between the first 10 amino acid residues of SecA (SecA2−11) with a model zwitterionic lipid bilayer, 1-palmitoyl-2-oleoyl-*sn*-glycero-3-phosphocholine (PC). To guide interpretation, SecA2−11 constructs were synthesized with three distinct geometries and multiple control experiments were carried out.[20] Repeated mechanical dissociation of SecA2−11 from PC generated dissociation force histograms also known as rupture force distributions, $P(F)$. Force data were connected to kinetic parameters via modeling the dissociation process as a diffusive escape over an energy barrier. Surprisingly, the SecA2−11 construct, a 10 amino acid long protein segment, exhibited complex dissociation behavior from PC bilayers including multiple kinetic pathways and catch bonding at certain pulling speeds.[21] Usually, increasing force loading on an intermolecular bond makes the bond rupture faster. However, the opposite occurs with a catch bond;[22] in this case, the lifetime of the bond increases with increasing force loading. Hence a relatively simple peptide-lipid interaction exhibited rich kinetic behavior. Activity of the Sec system depends on multiple contacts occurring at the cytoplasmic membrane interface, including protein−lipid interactions and protein−protein interactions (Figure 1).

The purpose of this work is to quantitatively characterize the interaction of SecA with *E. coli* membrane and to assess the possible biochemical implications. To gain traction on this complex system, we take a reductionist approach and focus on the N-terminal SecA-lipid interaction that directly impacts export function. Analysis was centered on the rupture event immediately before complete dissociation of the protein segment from the *E. coli* polar lipid bilayer, i.e., the last rupture event in each dissociation time series. Hence, we employed the first 10 amino acids of SecA (SecA2−11) rather than longer segments, such as the first 20 amino acids.[9] We found that the SecA2−11-*E. coli* polar lipid energy landscape was complex, comprising four dissociation pathways and catch bond behavior at certain pulling speeds. Yet, a well-defined protein−lipid dissociation rate in the absence of force was obtained. We note that our measurements do not account for the stabilization that likely occurs through direct contacts between SecA and the loops of SecY (i.e., the protein−protein interactions shown schematically in Figure 1).[5] We expect our results to represent a lower limit for the *in vivo* dissociation time. Characterizing this minimal system represents a step toward a more quantitative understanding of the interplay between SecA, the membrane surface, and SecYEG during the translocation process.

RESULTS AND DISCUSSION

We performed high precision (≤1 pN[23]) AFM-based dynamic force spectroscopy experiments to measure the strength of the interaction between the first 10 N-terminal amino acids of SecA and *E. coli* lipid bilayers (Figure 1). Tips were functionalized with SecA2−11 in a site-specific and covalent manner via a flexible linker,[24] allowing the peptide to orient freely while minimizing interactions with the surface of the AFM tip.[20] Supported lipid bilayers, robust mimics of cellular membranes, were employed.[25,26] The bilayer species was *E. coli* polar lipid which comprises a mixture of zwitterionic phosphoethanolamine ((PE), about 70 mol %) with charged phosphatidylglycerol ((PG), 20 mol %) and cardiolipin (a covalent PG dimer, 10 mol %). A 100% zwitterionic bilayer, PC, was also employed for reference. Figure 1c shows data as SecA2−11 was mechanically dissociated from the *E. coli* polar lipid bilayer by the AFM tip. The magnitude of the last rupture force (Figure 1c, arrow) was recorded for statistical analysis.

Dissociation Force Distribution Depends on Lipid Species. Figure 2a shows a kernel density estimate (smooth histogram) of the experimental (red line) rupture force distribution, $P(F)$, for SecA2−11 interacting with a supported *E. coli* polar lipid bilayer. Analogous data for the 100% zwitterionic reference PC is shown (Figure 2b[20,21]). In both cases, the theoretical modeling of $P(F)$ from the AFM measurements required four dominant dissociation pathways, corresponding to two single (n = 1, 2) and two double (n = 3, 4) rupture events. Following previous work,[21] we assigned the two single rupture pathways to the first two residues (i.e., L and I) at the N-terminus of SecA2−11 (Figure 2c,d), and regard the double rupture pathways as two consecutive single ruptures with time separation that cannot be resolved in the AFM measurement. The residues involved in double ruptures may come from the end region of either the same peptide (Figure 2e) or two separate copies of SecA2−11 attached to the tip of the AFM cantilever (Figure 2f).[21] Here, the activation energy, $\Delta G_n^{\ddagger}$, and distance to the transition state, $\Delta x_n^{\ddagger}$, have well-defined values inferred from the free energy profiles of residues I and L interacting with a PC bilayer, obtained in MD studies.[27,28] For *E. coli* lipid, we used the same parameter values as in PC because *E. coli*. membrane is mostly zwitterionic (~70%) and there are no free energy data

https://dx.doi.org/10.1021/acs.langmuir.9b03606
Langmuir 2020, 36, 2143−2152

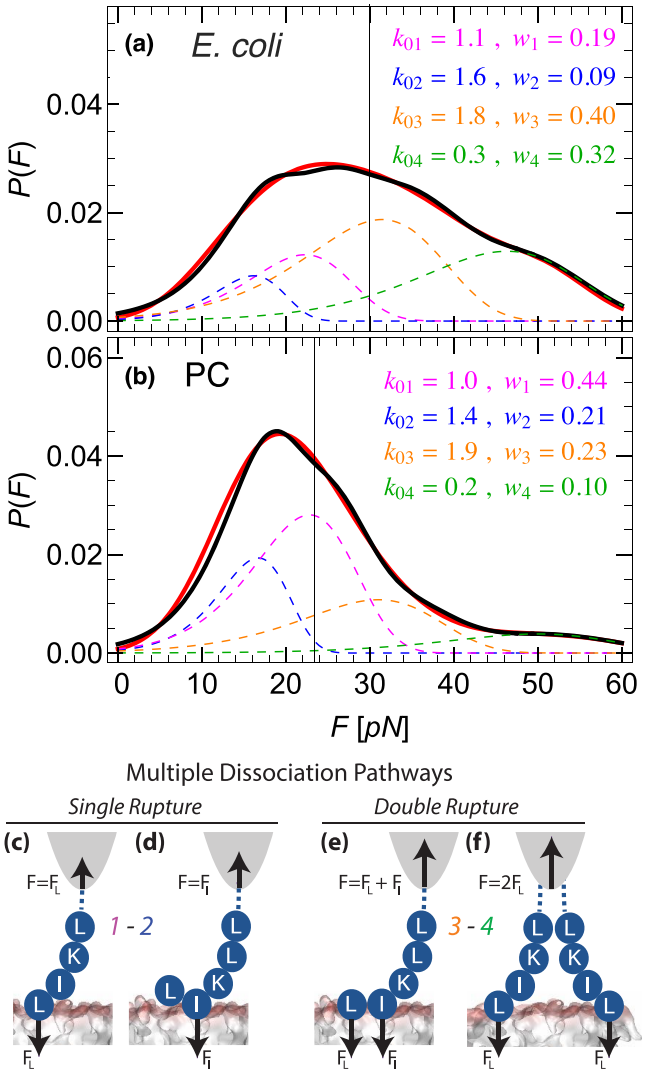

Figure 2. Force spectroscopy data and analysis overview. (a) Experimental (solid red line) dissociation force distribution $P(F)$ and theoretical model (solid black line) for SecA2−11 with *E. coli* polar lipid at a retraction speed of 100 nm/s (number of dissociation events, N_e = 261; number of distinct tips, N_t = 9). The theoretical $P(F)$ required four model force distributions (colored dashed lines) corresponding to four distinct dissociation pathways. For each pathway (n = 1, ..., 4), the intrinsic rupture rate, k_{0n} (units: 1/s), and statistical weight, w_n, are listed. The vertical line indicates the mean rupture force. (b) Data for SecA2−11 with PC lipid at a retraction speed of 100 nm/s is shown for reference (N_e = 286; N_t = 5). The model accounts for the two single-residue rupture pathways, shown in (c) and (d), and for two double-residue rupture pathways, involving either (e) two amino acid residues from the same single peptide rupturing simultaneously on the time scale of the measurement or (f) amino acids from two distinct peptides tethered near the apex area on the tip.

currently available for the amino acid residues in *E. coli* membrane.

The experimental $P(F)$ is well fit by the theoretical model with N = 4 dissociation pathways (Figure 2a,b, black lines). The activation energy, $\Delta G_n^{\ddagger}$, and distance to the transition state, $\Delta x_n^{\ddagger}$ were held fixed (see Materials and Methods for details) and the values of the fitting parameters k_{0n} and w_n, (for n = 1, ..., 4), are listed in the figure. The corresponding individual distributions $P_n(F)$ are plotted as colored dashed curves. Each k_{0n} corresponds to the effective off-rate for each dissociation pathway enumerated by index n, whereas the parameters w_n correspond to the statistical weight of each pathway. $P(F)$ is significantly broader in the case of the anionic *E. coli* lipid (mean rupture force $\bar{F}$ = 30 pN) than for the zwitterionic PC bilayer ($\bar{F}$ = 23 pN). Indeed, the full width at half-maximum of the *E. coli* distribution is nearly 2-fold larger than the PC distribution. The reason for this is that dissociation pathways exhibiting double rupture events (with higher rupture forces) are more abundant for *E. coli* lipid (>70%) than for PC (<35%). Electrostatic effects could be responsible for the dramatic increase of double rupture pathways observed in *E. coli* polar lipid when compared to PC. In addition, the increase could be related to secondary structure that the peptide adopts when binding to the membrane. Protein structure, if present, could give extra rigidity to the peptide that would favor the (almost) simultaneous dissociation of two residues. To further evaluate this, experiments were carried out to probe the secondary structure of the peptide when exposed to lipid.

Secondary Structure Varies with Lipid Species. We used far-UV circular dichroism (CD) spectroscopy to investigate the secondary structure of SecA2−11 in the presence and absence of varying concentrations of PC and *E. coli* polar lipids. Our CD data (Figure 3) support the existence

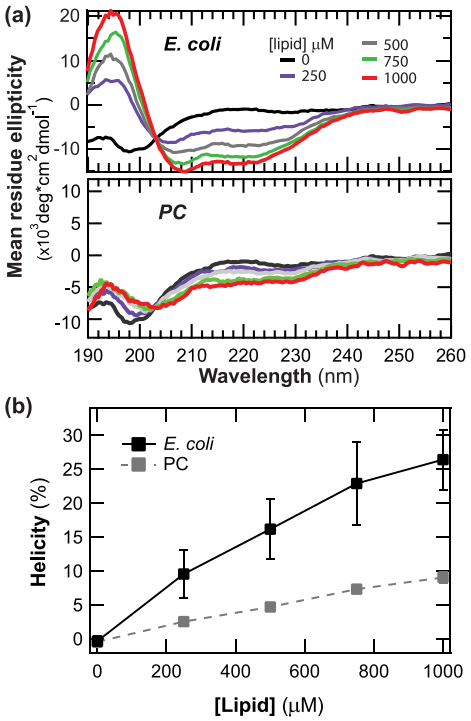

Figure 3. Secondary structure of SecA2−11. (a) Circular dichroism spectra for SecA2−11 in the presence of increasing concentration of *E. coli* polar liposomes (upper panel) or PC liposomes (lower panel). (b) Estimated helical content in *E. coli* polar lipid. The percent helix for SecA2−11 titrated with PC is shown for comparison (dashed).

of a significant conformation change in response to the presence of *E. coli* polar lipids based on three lines of evidence: (i) the CD spectrum at maximum lipid concentration (Figure 3a, upper panel, red) contains wavelength-specific maxima and minima that are indicative of the presence of α-helical structure; (ii) the presence of an isodichroic point at 203

https://dx.doi.org/10.1021/acs.langmuir.9b03606
Langmuir 2020, 36, 2143−2152

nm as the lipid concentration increases is consistent with a two-state transition from a disordered conformation to helical structure; (iii) partitioning analysis reveals the acquisition of helical structure as the lipid concentration increases.

First, inspection of the spectrum for SecA2−11 in 1 mM *E. coli* lipid (Figure 3a, upper panel, red) reveals a strong positive band at 193 nm, a strong negative band at 208 nm, and a weaker negative band at 222 nm. These three bands are characteristic of α-helical proteins and polypeptides.[29] Molecules with β structure will produce a positive band at 195 nm and negative band at 218 nm, so we cannot rule out the presence of β structure in the peptide.[30] In contrast the dominant trait of the peptide spectrum in aqueous buffer is a negative band at 195 nm, which is typical of a random coil, or disordered conformation.[31] The spectra for SecA2−11 in PC liposomes (Figure 3a, lower panel) undergo much smaller changes to those observed in *E. coli*.

Second, inspection of the upper panel of Figure 3a reveals that all five spectra cross at ∼203 nm, forming an isodichroic point. In general, such points indicate the presence of a two-state transition lacking stable intermediates. An isodichroic point at 203 nm is specifically associated with a two-state transition state from a random coil to a helical structure in proteins.[32] Note that SecA2−11 also shows an isodichroic point in PC lipids, consistent with a two-state transition, albeit one much smaller than that observed for *E. coli* polar lipid.

Finally, analysis of the spectra (Figure 3b) indicates that the average helical content of SecA2−11 increased from negligible in the absence of lipid to a maximum of about 26% in 1 mM *E. coli* polar lipid. In contrast, helical content only increased to about 9% in 1 mM PC (Figure 3b, gray markers and dashed line). These results are consistent with the spectral analyses described above as well as molecular dynamics simulations described below.

Hence, the aforementioned double rupture pathways which were observed in *E. coli* polar lipid at 100 nm/s retraction speed (Figure 2a) are likely due, at least in part, to the presence of secondary structure elements in the peptide. At the same time, the lower secondary structure content for SecA2−11 in PC is consistent with the smaller contribution to $P(F)$ of double rupture pathways observed at the same pulling speed in the 100% zwitterioinic lipid.

Loading Rate Dependence of *P*(*F*). Figure 4 shows the experimental $P(F)$ (red lines) for SecA2−11 interacting with *E. coli* polar lipid bilayers for four different retraction speeds of the base of the AFM cantilever away from the membrane, v = 50, 100, 200, and 300 nm/s. It is remarkable that, in spite of the strong speed dependence of $P(F)$, the rupture force distributions were fit well (black lines) by using the same four dissociation pathways identified above. Note that, apart from minor adjustment of the intrinsic dissociation rates for the double rupture pathways, the fitting simply required the recalculation of the weight factors w_n. For retraction speeds v < 300 nm/s, the contribution to $P(F)$ of the double rupture pathways dominated (>50%). However, at the highest pulling speed v = 300 nm/s, this contribution decreased below 40%, and single rupture pathways dominated.

Intrinsic and Force Dependent Off-Rate from the Membrane. The force dependent dissociation rate, $k(F)$, of SecA2−11 from *E. coli* polar lipid can be calculated in model independent fashion directly from the experimental distribution of rupture forces $P(F)$ (eq 1, Materials and Methods). The results are shown in Figure 5. The strong velocity

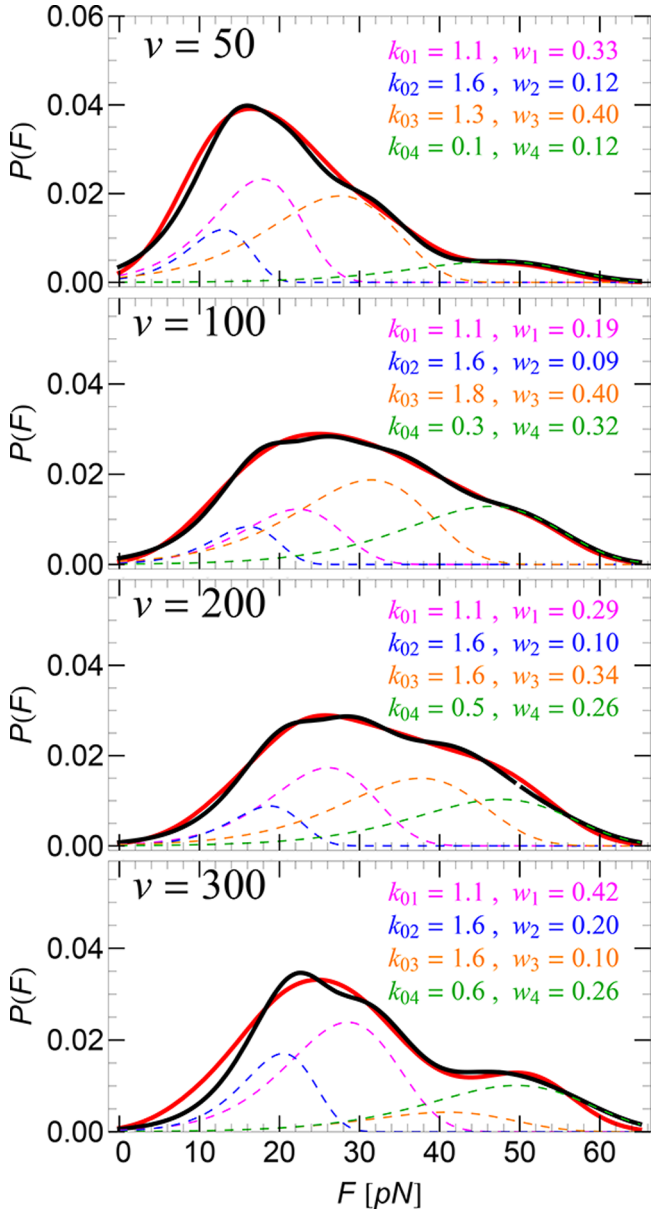

Figure 4. Retraction speed dependence of $P(F)$ for SecA2−11 in *E. coli* polar lipid. The experimental results (solid red curves) are matched well by the theoretical model (solid black curves) by using four dissociation pathways. Contributions to $P(F)$ from the individual pathways are shown as colored dashed curves; the corresponding intrinsic rupture rates, k_{0n}, and weights, w_n, (with n = 1···4) are also listed. For the four retractions speeds, the total number of events, aggregated from N_t = 3, 9, 7, and 6 distinct tips, were, respectively, N_e = 64, 261, 236, and 79.

dependence and nonmonotonic behavior of $k(F)$ is a clear indication that this dissociation is a multiple pathway process.[21] Furthermore, $k(F)$ exhibited catch bond behavior,[21] where counterintuitively, the dissociation rate decreased with increasing applied force.[22,33,34] In particular, a catch bond region is manifest in the v = 300 nm/s curve in Figure 5 (at F ≈ 35 pN) where the slope of the $k(F)$ versus F curve is negative.

In spite of the significant pulling speed dependence of $k(F)$, we found that the intrinsic (dissociation) off-rate of SecA2−11 from *E. coli* polar lipid, $k_0 = k(0) = \sum_{n=1}^{4} w_n k_{0n}$, was

https://dx.doi.org/10.1021/acs.langmuir.9b03606
Langmuir 2020, 36, 2143−2152

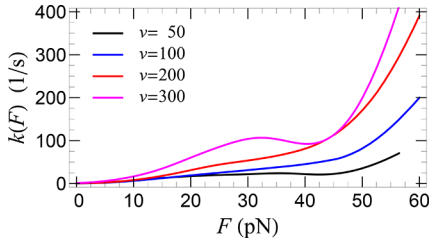

Figure 5. Force dependent dissociation rate, $k(F)$, of SecA2−11 from *E. coli* polar lipid, for the listed retraction speeds (in nm/s) of the base of the AFM cantilever. Note that the negative slope region of the $k(F)$ curve, indicative of catch-bond behavior, is prominent in the vicinity of 35 pN for the 300 nm/s data (magenta).

essentially independent of pulling speed, as shown in Figure 6. The intrinsic off-rate that we obtained here, k_0 = 1.13 ± 0.04

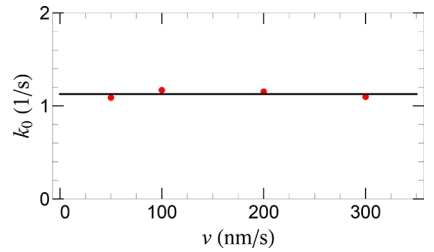

Figure 6. AFM retraction speed, v, dependence of the intrinsic dissociation rate, $k_0 = k(F = 0)$, (red filled-circles) of SecA2−11 interacting with *E. coli* membrane. Horizontal black line represents the mean value $\bar{k}_0$ = 1.13 s^{-1}.

s^{-1} (mean ± standard deviation), is about 12% lower than that for the same peptide interacting with a PC bilayer (k_0 = 1.27 ± 0.09 s^{-1}).[21]

Conformational Dynamics of SecA2−11 in Lipid Membranes. Molecular dynamics (MD) simulations were performed to corroborate the experimental data and provide additional conformational details. To explore the limiting cases, two membrane systems were set up, one composed of 100% anionic PG lipid and the other 100% zwitterionic PC. Because PC exhibits similar physical properties to PE, in principle, a linear combination of these results can be used to approximate the behavior of the *E. coli* polar lipid mixture.

Two 0.5 μs long MD trajectories of the PC and PG systems provide insight, at the atomistic level, into the partitioning of SecA2−11 from solution to lipid bilayers. In both simulations (Figure 7), the peptide associates spontaneously with the bilayers on a time scale of 100 ns. To quantify the degree of penetration of the peptide in the membrane, one calculates the position of its center of mass (COM), $\Delta z(t)$, relative to the surface of the membrane, i.e., along the membrane normal z direction. The surface of the membrane is defined as the planar surface determined by the P atoms in the appropriate leaflet. The time evolution of the peptide-membrane separation, $\Delta z(t)$, in both PC and PG, is plotted (Figure 7a). As expected, the results show that the COM of the positively charged peptide penetrates deeper in the neutral PC than in the anionic PG bilayer.

After 300 ns, both systems appear to be equilibrated, with the COM of SecA2−11 fluctuating about a mean level located slightly below (above) the surface of the PC (PG) membrane. Thus, while SecA2−11 in PG is located mostly in the headgroup region, in PC, it penetrates deeper into the

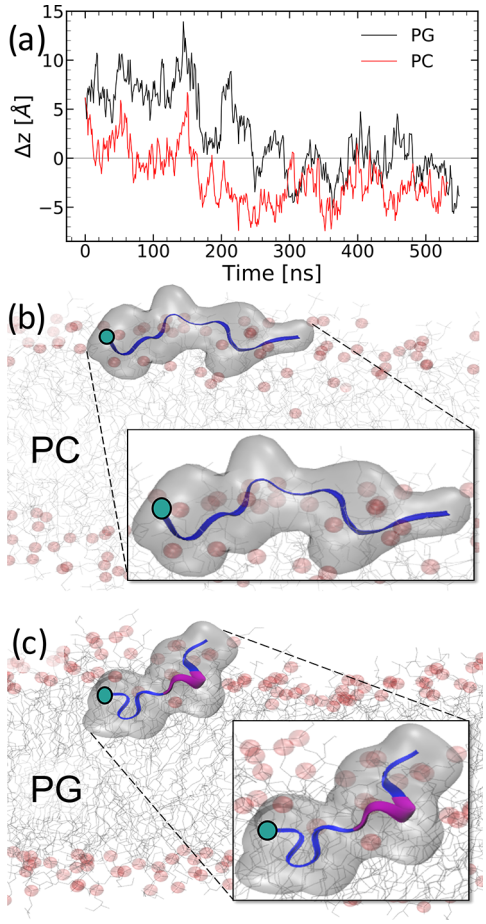

Figure 7. (a) Time evolution of the position, along the z-axis, of the COM of SecA2−11 relative to the surface of the membrane (defined by the mean position of the P atoms, which was set as origin, z = 0) in both PC (black line) and PG (red line). Representative snapshots of (b) PC and (c) PG taken, respectively, at 350 and 360 ns. The backbone of the peptide is shown in cartoon representation and is colored according to secondary structure (magenta for 3_{10} helix and blue for random coil). The transparent surface representation indicates the spatial extent of SecA2−11. The P atoms in the headgroup of the lipids are shown as red spheres, and for clarity, water molecules were omitted. The location of AFM tip tether is indicated (green dot). All snapshots were rendered using VMD.[35]

hydrophobic core of the membrane. This result is consistent with the fact that the electrostatic interaction between the peptide and membrane is stronger in PG than in PC (see Table 1). Furthermore, due to the stronger peptide-membrane interaction, SecA2−11 has a more compact configuration in PG than in PC (Figure 7, compare panels b and c), consistent with its smaller solvent-accessible-surface-area (SASA) and radius of gyration (Table 1).

Table 1. Electrostatic Interaction Energy (E_{es}), Solvent Accessible Surface Area (SASA), and Radius of Gyration (R_g) of SecA2-11 in PC and PG Obtained from MD Simulations

System	E_{es}[kcal/mol]	SASA [Å^2]	R_g [Å]
PC	−258 ± 82	1712 ± 57	8.5 ± 0.5
PG	−294 ± 102	1645 ± 57	7.3 ± 0.7

https://dx.doi.org/10.1021/acs.langmuir.9b03606
Langmuir 2020, 36, 2143−2152

In PC, just like in solution, SecA2−11 exhibits a random coil configuration with no secondary structure.[20] Conversely, in PG, SecA2−11 acquires intermittent, partial 3_{10} helical structure. Indeed, by using the DSSP[36] algorithm for secondary structure assignment, we have found that in PC all SecA2−11 residues are part of a random coil, whereas in PG three residues (K4, L5 and L6), intermittently, form a turn of a 3_{10} helix. These MD simulation results are in general agreement with circular dichroism measurements (Figure 3), according to which SecA2−11 exhibits little to no secondary structure in PC, while it acquires a substainitial fraction of helical structure in *E. coli* polar lipid, most likely due to its PG lipid content. A more precise quantitative description of the penetration of the peptide in a membrane is to specify the mean position, Δz, of each residue (identified, e.g., through the C_α atom) with respect to the surface of the membrane. The Δz values for the ten SecA2−11 residues in both PC and PG, obtained from the MD simulations, are shown in Figure 8a. Also, while the Δz values for the five residues from the C-terminus are similar in both PC and PG, these values for the five residues from the N-terminus are noticeably larger in PG than in PC. This result is consistent with the time evolution of the distance of the COM of SecA2−11 from the surface of the two bilayers shown in Figure 7.

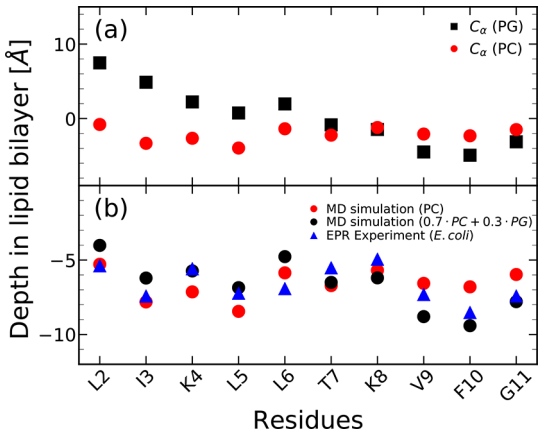

Figure 8. (a) Mean penetration depth, Δz, of the SecA2−11 amino acids (measured with respect to the plane of the P atoms) in PC and PG, expressed in terms of the position of their C_α atom. (b) Comparison between EPR experiment[37] (triangles) and MD simulation (circles) results for Δz of the SecA2−11 amino acids. The −4 Å overall shift applied to the MD data is comparable to the uncertainty in defining the position of the membrane surface. The MD data correspond to SecA2−11 in PC (red circles) and an *E. coli* polar lipid mimic (black circles), determined as a weighted average of the PC (70%) and PG (30%) results.

Comparison with EPR Study of Full Length SecA. In a recent experimental study of the interaction between SecA with *E. coli* lipid, the penetration depth of the ten amino terminal residues corresponding to SecA2−11 within full length SecA was measured via power saturation electron paramagnetic resonance spectroscopy (EPR).[37] As shown in Figure 8b, the experimentally measured Δz values appear to be in general agreement with our MD simulation results for PC and also for an *E. coli* membrane mimic for which Δz was calculated as a weighted average for PC (70%) and PG (30%). Note that the MD results were subject to a −4 Å overall shift, which is comparable to the size of the phosphate group and, thus, to the uncertainty in defining the position of the membrane surface.

CONCLUSIONS

We studied the critical SecA-lipid bilayer interaction that underlies protein export activity in *E. coli*. Our mechanical approach, based on direct and precise measurements of the force experienced by the extreme N-termial 10 amino acids of SecA, revealed several interesting features in a complex energy landscape. Recent EPR measurements validate the approach.

Findik and co-workers[37] measured the penetration depth of full length SecA in *E. coli* polar lipid. Their results are in general agreement with our MD results using the SecA2−11 peptide (Figure 8). This suggests (i) that the N-terminus of SecA acts as an independent lipid-binding entity, consistent with other work in the field,[9,10] and (ii) probing the interaction between *E. coli* polar lipid and the N-terminal 10 amino acids of SecA provides insight into biochemically meaningful binding activity. Hence, the overall methodology is supported by this agreement.

Single molecule force spectroscopy experiments uncovered complex multimodal dissociation force distributions. To extract intrinsic kinetic parameters from these data, we applied a recently developed theory based on the coexistence of multiple stochastic dissociation pathways.[20,21] Four prominent dissociation pathways corresponding to two single and two double rupture events with varying statistical weights were required to model the AFM data. We note that the inclusion of double rupture pathways in the analysis[21] improves upon our previous work in which only two single rupture pathways were considered.[20] The new analysis accounts not only for the possibility of two amino acid residues from the same single peptide rupturing simultaneously (Figure 2e) but also for the difficult-to-experimentally control possibility of >1 peptide affixed to the AFM tip apex (Figure 2f). Counterintuitive catch bond behavior, wherein the stronger the applied force, the longer lived the bond became, was evident (Figure 5). Despite complicating factors, kinetics analysis converged to a well-defined mean off-rate in the absence of force. In particular, we determined $k_0 = 1.13 \pm 0.04\ s^{-1}$ for SecA2−11 dissociating from an *E. coli* polar lipid bilayer (Figure 6).

How does this time scale compare to the that of the secretion process itself? The complexity of the general secretory system has obfuscated central facets, including the fundamental nature of the translocation mechanism. "Power-stroke", "Brownian ratchet", and other mechanisms have been proposed,[1,2,9,38] and recent experiments have shown aspects of the process that vary with precursor species.[39−41] What is clear is that proteins are generated at bacterial ribosomes at a rate of ≈20 amino acids per second.[42] Measured rates for SecA-driven translocation of the precursor of outer membrane protein A through SecYEG range from about 5 to 40 amino acids per second.[43−45] The mean bound-state lifetime from our dynamic force spectroscopy experiments of SecA2−11 and *E. coli* polar lipid was $\tau_0^{lipid} = k_0^{-1} \approx 0.9$ s. This implies that lipid interactions alone could keep SecA engaged on the membrane for a time period commensurate with the translocation of on average ∼20 amino acid residues. We note that the operational unit of the protein transportation apparatus has been reported to proceed in steps of ∼25 amino acid residues.[46] Our result is likely to represent a conservative lower limit for the *in vivo* membrane-bound-state lifetime because our measurements do not account for intermediate rupture events or for translocase

https://dx.doi.org/10.1021/acs.langmuir.9b03606
Langmuir 2020, 36, 2143−2152

stabilization that likely occurs through direct SecA-SecY contacts (Figure 1).[4,5] Precursor mediated contacts and additional SecA-lipid interactions beyond the extreme N-terminal residues are also possible.[9,47] However, allosteric destabilization of the translocase complex is a formal possibility as well.

Our experiments revealed that the stability of the SecA-lipid interaction likely comes about, at least in part, from the formation of secondary structure when the extreme N-terminal region of SecA contacts *E. coli* polar lipid bilayers. Comparative analysis of rupture force distributions at the same pulling speed (Figure 2) indicated a roughly 2-fold enhancement of double rupture pathways commensurate with a 12% bound-state lifetime enhancement for *E. coli* lipid over PC lipid. In terms of the physical origin of these distinctions, electrostatics (e.g., monopole versus dipole interactions) likely play a direct role. Additionally, the data indicate an attendant increase in SecA2−11 helical content in polar lipid environments over zwitterionic lipid. MD predicted residues K4, L5, and L6 exhibit helical structure in polar lipid; these residues are immediately proximal to the two extreme N-terminal residues (L2 and I3). Because a structured peptide would be more mechanically rigid and exhibit a longer persistence length, we posit that it would be more likely to simultaneously (on the mechanical response time scale of the measurement, 0.1 ms[48]) dissociate multiple residues compared to an unstructured peptide when subject to the same pulling conditions. We also note that the rigidity of the lipid-bound polypeptide segment may play a role in propagating conformational changes to membrane-distal regions of SecA that influence translocation activity.[10]

In summary, we quantitatively characterized the locus of a peripheral membrane protein−lipid bilayer interaction underlying protein transportation activity in *E. coli*. The methods demonstrated here could potentially be applied to phospholipid binding sites in a range of peripheral membrane protein systems of interest. Further work is needed to develop methodology for interpreting intermediate rupture events which could be employed, for example, to study lipid interactions with longer polypeptides.

MATERIALS AND METHODS

Force Spectroscopy Experiments. To achieve $\lesssim$1 pN level precision, bioloever long cantilevers (Olympus) were treated in gold etchant followed by chromium etchant (Transene). This process removes all metalization.[23,48] Cantilever spring constants (k_s) were in the range of 3−8 pN/nm, determined via the thermal calibration. SecA2−11 with sequence LIKLLTKVFG-C was synthesized in house (purity ≥95%) using solid-phase synthesis on Sieber amide resin and standard Fmoc/*t*Bu chemistry for linear elongation. The cysteine residue at the C-terminus allowed site-specific, covalent functionalization onto AFM tips via a 9.5 nm long PEG linker. For functionalization, cantilevers were plasma cleaned (10 min, 30 W, Harrick Plasma), immersed in silane (3-ethoxydimethylsilyl) propylamine (Sigma-Aldrich) for 60 s, and baked at 80 °C for 30 min. These dry tips were incubated in sodium borate (50 mM, pH 8.5) for 1 h, followed by NHS-PEG_{24}-maleimide (Thermo Scientific) for 1 h, and then peptide at 100 μM for 2 h. Finally, tips were washed (75 mM Na_3PO_4, pH 7.2) and loaded into the microscope for force spectroscopy experiments. Such conditions yield ∼1 peptide tethered to the tip apex.[20] PC and *E. coli* polar lipid extract were purchased (Avanti Polar Lipid). Liposomes were prepared by extrusion (50 mM sodium phosphate pH 7.2, 50 mM NaCl, 10 mM ethylenediaminetetraacetic acid) through a membrane (approximately 25 times, 100 nm pore diameter). Supported lipid bilayers were formed by vesicle fusion (70 μM, 30 min incubation, ∼30 °C) to clean glass surfaces. Such conditions result in uniform bilayer coverage over large areas.[26,49,50] All force spectroscopy experiments were carried out in aqueous buffer solution (10 mM Hepes pH 7.6, 300 mM KAc, 5 mM $Mg(Ac)_2$) at ∼30 °C using a commercial AFM (Cypher, Asylum Research). The retraction speed, v, was controlled by the piezoelectric stage affixed to the base of the cantilever. To minimize artifacts, during all experiments, the greatest compressive force applied to the lipid bilayer was ∼100 pN. Dissociation events exhibiting rupture forces >60 pN were rare and excluded from analysis. Additionally, events occurring <3 nm above the lipid surface were excluded from analysis.

Computer Modeling and MD Simulations. A completely extended, atomistic model of the peptide SecA2−11 (LIKLLTKVFG-C) was built using the Molefacture plugin in the molecular visualization and the modeling software VMD.[35] To closely mimic the experimental system in which the peptide is covalently bonded through a Cys residue to a PEG linker attached to a functionalized AFM tip, a Cys residue was added to the C-terminus of SecA2−11.[20] Two model systems were built by placing a copy of the peptide parallel to the surface of fully solvated (and pre-equilibrated) lipid bilayers made, respectively, of zwitterionic POPC lipids (system PC) and anionic POPG lipids (system PG). Each bilayer contained 128 lipids (64 lipids per leaflet). The PC bilayer was built using the Membrane plugin in VMD[35] and solvated with 5895 TIP3P water molecules, while the PG bilayer was built in CHARMM-GUI[51,52] and solvated with 4971 TIP3P waters. Using the Autoionize plugin in VMD, system PC (PG) was neutralized by adding 2 Cl^- (2 Cl^- and 128 K^+) counterions. Finally, the PC (PG) system comprised a total of 35030 (31490) atoms and (after equilibration) occupied an orthorhombic unit cell with dimensions 72 × 64 × 72 $Å^3$ (72 × 64 × 66 $Å^3$).

MD simulations were performed with NAMD2.12,[53] using the CHARMM36 force field parameters,[54,55] and employing periodic boundary conditions. The MD equations of motion were integrated with a multiple time stepping scheme with the r-RESPA algorithm. The time steps were, respectively, 1, 2, and 4 fs for bonded, short-range (van der Waals) and long-range (electrostatic) interactions. Van der Waals interactions were cut off at 12 Å with a smooth switching function starting at 10 Å. Long-range electrostatic interactions were computed with the Particle Mesh Ewald (PME) method, with a grid spacing of 1 Å.

After energy minimization and several stages of equilibration, 0.5 μs long production runs of equilibrium MD in the *NPT* ensemble were performed with both PC and PG. The temperature was kept constant at T = 300 K by using a Langevin thermostat with a damping coefficient of 1 ps^{-1}. The pressure was maintained at normal value (P = 1 atm) by employing the Nosé−Hoover Langevin piston barostat with period of 100 fs and decay time of 50 fs.

In order to mimic the supported lipid membranes used in the AFM experiments, the phosphorus (P) atoms from the lower leaflet of the phospholipid bilayer in both PC and PG systems were harmonically restrained during the MD simulations, thus preventing the drift of the membrane along the z-direction, normal to its plane. We have verified that the applied restrains did not alter the dynamics and behavior of the systems, as no noticeable change of the bilayer thickness, the density profile of P (and other lipid) atoms, or the acyl chain order parameter were observed.

The MD simulations were carried out on several GPU accelerated workstations equipped with 36 Intel Xeon CPUs cores, with a performance of around 36 ns/day. All analyses of the MD simulations were performed with MDAnalysis,[56,57] MDTraj,[58] and VMD.[35]

Circular Dichroism Spectroscopy. CD spectroscopy was performed to evaluate the secondary structural content of the SecA2−11 peptide in solution and in contact with lipids. A JASCO J-815 spectrophotometer was used. Spectra were recorded from 190 to 260 nm using a 1 mm path length quartz cuvette in a thermostated sample compartment maintained at 8 °C. The step-size was 0.5 nm, the bandwidth was 1 nm, the scan rate was 20 nm/min. The averaged spectra were smoothed using a five-point moving average algorithm. Peptide concentration was 45 μM, and total lipid concentration varied between 0 and 1000 μM. Constant pH was maintained using 10 mM

https://dx.doi.org/10.1021/acs.langmuir.9b03606
Langmuir 2020, 36, 2143−2152

Tris, pH 7.6 buffer. The percent of helical structure was estimated by measuring the mean residual ellipticity (MRE) at 222 nm, the wavelength where pure α helical structure has its maximum negative absorbance. Using known values for 0% and 100% helical structure obtained from reference spectra,[59,60] the percent helical content can be determined according to the following equation

$$\textit{Percent helical structure} = \frac{(\theta_{exp} - \theta_{0\%})}{(\theta_{100\%} - \theta_{0\%})} \times 100\%$$

where θ_{exp} is the MRE value at 222 nm from an experimental spectrum, $\theta_{0\%}$ is the value at 222 nm in the absence of helical structure, and $\theta_{100\%}$ is the value for a completely helical structure. The reference values of −3000 (mdeg·cm^2)dmol^{-1} for 0% helical and −39500 (mdeg·cm^2)dmol^{-1} for 100% helical[61] were modified to −1066 and −37566 (mdeg·cm^2)dmol^{-1}, respectively, to account for local instrumentation. Values reported are the average of four separate experiments for the *E. coli* polar lipids and three separate experiments for the PC liposomes; standard deviations are provided.

Theoretical Modeling of *P*(*F*) and *k*(*F*). Here, we summarize the theoretical modeling approach used in this work; further details can be found in our previous work.[21] While the dissociation force histogram, $P(F)$, can be easily built from precision AFM dynamic force spectroscopy measurements, the direct experimental determination of the corresponding force dependent rupture rate, $k(F)$, is more challenging. In general, $k(F)$ can be calculated, in a model independent manner, from $P(F)$ and the experimentally tunable force loading rate $\dot{F} = k_s v$, where k_s and v are, respectively, the effective stiffness of the AFM cantilever and the retraction speed. Indeed[21,62,63]

$$k(F) = \frac{\dot{F}P(F)}{\int_F^\infty P(f)df} \tag{1}$$

Similarly, by inverting eq 1, $P(F)$ can also be expressed[21,62,63] only in term of $k(F)$ and $\dot{F}$

$$P(F) = \frac{k(F)}{\dot{F}} \exp\left[-\int_0^F \frac{k(f)}{\dot{F}} df\right] \tag{2}$$

As any biomolecular rupture event, peptide-lipid membrane dissociation can be described as a diffusive escape process across a free energy barrier, along the reaction coordinate x, defined as the separation between the peptide and the membrane.[62,64−66] The stochastic model for such single pathway dissociation process is characterized by three parameters, namely the (i) activation energy (height of the intrinsic free energy barrier), $\Delta G_0^{\ddagger}$; (ii) activation length (distance between the bound and transition states), $\Delta x_0^{\ddagger}$; and (iii) intrinsic escape rate, k_0. We model the free energy profile (*potential of mean force* or PMF) by the widely used linear-cubic potential $U_0(x) = \Delta G_0^{\ddagger}[(3/2)(x/\Delta x_0^{\ddagger}) - 2(x/\Delta x_0^{\ddagger})^3]$, which was shown to be suitable for studying forced dissociation processes.[62] The applied dissociation force, F, alters the values of the model parameters. As F increases, both $\Delta G^{\ddagger}(F)$ and $\Delta x^{\ddagger}(F)$ decrease, while $k(F)$ increases. In terms of the force altered PMF, $U(x) = U_0(x) - Fx$, the force dependent rupture rate can be calculated as the inverse of the mean first passage time[21,67]

$$k(F) = k_0 \frac{\int_{-\Delta x_0^{\ddagger}/2}^{\Delta x_0^{\ddagger}/2} dx\, \exp[\beta U_0(x)] \int_{-\infty}^{x} dy\, \exp[-\beta U_0(y)]}{\int_{-\Delta x^{\ddagger}/2}^{\Delta x^{\ddagger}/2} dx\, \exp[\beta U(x)] \int_{-\infty}^{x} dy\, \exp[-\beta U(y)]} \tag{3}$$

where $\beta = 1/k_B T$, with k_B, the Boltzmann's constant, and T, the absolute temperature.

In principle, the three model parameters can be determined by either fitting directly eq 3 to the experimental $k(F)$ from eq 1, or by inserting eq 3 into eq 2 and fitting the resulting rupture force distribution to the experimental force histogram $P(F)$. It should be emphasized that because $k(F)$ in eq 3 is (i) independent of the retraction speed v (or, equivalently, the force loading rate, $\dot{F}$) and (ii) increases monotonically with F, the single pathway model cannot describe peptide-lipid membrane dissociation processes in which $k(F)$, obtained in model independent fashion from the experimental $P(F)$ histogram [through eq 1], is manifestly v dependent and nonmonotonic.[21]

Recently, we have shown that peptide-lipid membrane dissociation occurs stochastically along a few (usually N = 3 or 4) dominant pathways.[21] Although the relative frequency (probability) w_n of the individual pathways cannot be predicted (they change from experiment to experiment even for the same system), each pathway can be uniquely characterized by the three model parameters $\Delta G_n^{\ddagger}$, $\Delta x_n^{\ddagger}$. and k_{0n}, n = 1, ..., N. Furthermore, for each pathway, $k_n(F)$ can be calculated using eq 3, which inserted into eq 2 yields $P_n(F)$. Finally, in the multiple dissociation pathways model[21]

$$P(F) = \sum_{n=1}^{N} w_n P_n(F) \tag{4a}$$

and

$$k(F)^{-1} = \sum_{n=1}^{N} c_n(F) k_n(F)^{-1}$$

$$\text{with} \quad c_n(F) = w_n \frac{P_n(F)}{P(F)} \tag{4b}$$

We have also shown that, in general, the individual dissociation pathways correspond to either single or double amino acid rupture events.[21] Single ruptures usually involve either the last (Figure 2c) or next to last residues (Figure 2d). Double ruptures are two single ruptures that occur in rapid succession, which cannot be resolved experimentally, and may involve two residues located at the end region of either one (Figure 2e) or two peptides attached to the same AFM tip (Figure 2f). We note that modeling $P(F)$ from individual tips required multiple pathways.[21] Additionally, four pathways account for the majority (≥97%), but in some cases, not all, of $P(F)$. The discrepancy corresponds to the difficult-to-sample portions of $P(F)$ and can be accounted for by additional pathways which occur less frequently. Finally, note that while for individual pathways the intrinsic rates, k_{0n}, show only weak membrane species dependence, the weight coefficients, w_n, may vary considerably, likely due to the complex nature of peptide-lipid membrane interactions.

The steps involved in modeling $P(F)$ and $k(F)$ obtained in the AFM measurements are as follows. First, one identifies two single dissociation pathways corresponding to the last two residues at the end of the peptide SecA2−11, i.e., L and I, which are most likely to rupture last. Double rupture pathways, involving two of these residues, are also considered. Next, the corresponding activation energies and lengths are identified from MD studies,[27,28] i.e., $\Delta G_1^{\ddagger}$ = 8 kT and $\Delta x_1^{\ddagger}$ = 1.0 nm for L and $\Delta G_2^{\ddagger}$ = 10 kT and $\Delta x_2^{\ddagger}$ = 1.3 nm for I, respectively.[21] The activation energies and lengths, which depend on the nature of the peptide and lipid membrane, are treated as constants during the fitting process. The remaining parameters, namely, the intrinsic dissociation rates k_{0n} and weight coefficients w_n for each dissociation pathway (n = 1, ..., N) are determined by fitting the experimental $P(F)$ histograms.

AUTHOR INFORMATION

Corresponding Authors

Ioan Kosztin − *Department of Physics and Astronomy, University of Missouri, Columbia, Missouri 65211, United States*; Email: kosztini@missouri.edu

Gavin M. King − *Department of Physics and Astronomy and Department of Biochemistry, University of Missouri, Columbia, Missouri 65211, United States*; orcid.org/0000-0002-5811-7012; Email: kinggm@missouri.edu

https://dx.doi.org/10.1021/acs.langmuir.9b03606
Langmuir 2020, 36, 2143−2152

Authors

Tina R. Matin − *Department of Physics and Astronomy, University of Missouri, Columbia, Missouri 65211, United States*

Milica Utjesanovic − *Department of Physics and Astronomy, University of Missouri, Columbia, Missouri 65211, United States*

Krishna P. Sigdel − *Department of Physics and Astronomy, University of Missouri, Columbia, Missouri 65211, United States*

Virginia F. Smith − *Department of Chemistry, United States Naval Academy, Annapolis, Maryland 21402, United States*

Complete contact information is available at: https://pubs.acs.org/10.1021/acs.langmuir.9b03606

Author Contributions

[$]T.R.M. and M.U. contributed equally.

Notes

The authors declare no competing financial interest.

■ ACKNOWLEDGMENTS

The authors gratefully acknowledge Chunfeng Mao, Linda Randall, Stephen White, and Martin Ulmschneider for discussions as well as Gerald Hazelbauer and Leighanne Basta for critical reading of this manuscript. This work was supported by the Burroughs Wellcome Fund (Career Award at the Scientific Interface), the NSF (CAREER Award #: 1054832), and the MU Research Board. The computation for this work was performed on the HPC infrastructure provided by RCSS and in part by the NSF under grant number CNS-1429294 at the University of Missouri, Columbia MO.

■ REFERENCES

(1) Crane, J. M.; Randall, L. L. The Sec System: Protein Export in *Escherichia coli*. *EcoSal Plus* **2017**, *7*, 2017 DOI: 10.1128/ecosalplus.ESP-0002-2017.

(2) Tsirigotaki, A.; De Geyter, J.; Šoštaric, N.; Economou, A.; Karamanou, S. Protein Export through the Bacterial Sec Pathway. *Nat. Rev. Microbiol.* **2017**, *15*, 21−36.

(3) Lill, R.; Dowhan, W.; Wickner, W. The ATPase Activity of secA Is Regulated by Acidic Phospholipids, secY, and the Leader and Mature Domains of Precursor Proteins. *Cell* **1990**, *60*, 271−280.

(4) Mori, H.; Ito, K. An essential amino acid residue in the protein translocation channel revealed by targeted random mutagenesis of SecY. *Proc. Natl. Acad. Sci. U. S. A.* **2001**, *98*, 5128−5133.

(5) Zimmer, J.; Nam, Y.; Rapoport, T. A. Structure of a complex of the ATPase SecA and the protein-translocation channel. *Nature* **2008**, *455*, 936.

(6) Cabelli, R. J.; Dolan, K. M.; Qian, L. P.; Oliver, D. B. Characterization of membrane-associated and soluble states of SecA protein from wild-type and SecA51(TS) mutant strains of *Escherichia coli*. *J. Biol. Chem.* **1991**, *266*, 24420−7.

(7) Ulbrandt, N. D.; London, E.; Oliver, D. B. Deep Penetration of a Portion of *Escherichia coli* SecA Protein into Model Membranes Is Promoted by Anionic Phospholipids and by Partial Unfolding. *J. Biol. Chem.* **1992**, *267*, 15184−15192.

(8) Chen, X.; Brown, T.; Tai, P. C. Identification and Characterization of Protease-Resistant SecA Fragments: SecA Has Two Membrane-Integral Forms. *J. Bacteriol.* **1998**, *180*, 527−537.

(9) Bauer, B. W.; Shemesh, T.; Chen, Y.; Rapoport, T. A. A "push and slide" mechanism allows sequence-insensitive translocation of secretory proteins by the SecA ATPase. *Cell* **2014**, *157*, 1416−29.

(10) Koch, S.; de Wit, J. G.; Vos, I.; Birkner, J. P.; Gordiichuk, P.; Herrmann, A.; van Oijen, A. M.; Driessen, A. J. M. Lipids Activate SecA for High Affinity Binding to the SecYEG Complex. *J. Biol. Chem.* **2016**, *291*, 22534−22543.

(11) Koch, S.; Exterkate, M.; Lpez, C.; Patro, M.; Marrink, S.; Driessen, A. Two distinct anionic phospholipid-dependent events involved in SecA-mediated protein translocation. *Biochim. Biophys. Acta, Biomembr.* **2019**, *1861*, 183035.

(12) Yu, H.; Siewny, M. G. W.; Edwards, D. T.; Sanders, A. W.; Perkins, T. T. Hidden Dynamics in the Unfolding of Individual Bacteriorhodopsin Proteins. *Science* **2017**, *355*, 945−950.

(13) Muller, D. J.; Dufrene, Y. F. Atomic force microscopy: a nanoscopic window on the cell surface. *Trends Cell Biol.* **2011**, *21*, 461−469.

(14) Przybylo, M.; Sykora, J.; Humpolickova, J.; Benda, A.; Zan, A.; Hof, M. Lipid diffusion in giant unilamellar vesicles is more than 2 times faster than in supported phospholipid bilayers under identical conditions. *Langmuir* **2006**, *22*, 9096−9.

(15) Desmeules, P.; Grandbois, M.; Bondarenko, V. A.; Yamazaki, A.; Salesse, C. Measurement of membrane binding between recoverin, a calcium-myristoyl switch protein, and lipid bilayers by AFM-based force spectroscopy. *Biophys. J.* **2002**, *82*, 3343−50.

(16) Andre, G.; Brasseur, R.; Dufrene, Y. F. Probing the interaction forces between hydrophobic peptides and supported lipid bilayers using AFM. *J. Mol. Recognit.* **2007**, *20*, 538−45.

(17) Min, D.; Jefferson, R. E.; Bowie, J. U.; Yoon, T. Y. Mapping the energy landscape for second-stage folding of a single membrane protein. *Nat. Chem. Biol.* **2015**, *11*, 981−7.

(18) Schwierz, N.; Krysiak, S.; Hugel, T.; Zacharias, M. Mechanism of Reversible PeptideBilayer Attachment: Combined Simulation and Experimental Single-Molecule Study. *Langmuir* **2016**, *32*, 810−821.

(19) Ma, L.; Cai, Y.; Li, Y.; Jiao, J.; Wu, Z.; O'Shaughnessy, B.; De Camilli, P.; Karatekin, E.; Zhang, Y. Single-molecule force spectroscopy of protein-membrane interactions. *eLife* **2017**, *6*, No. e30493.

(20) Matin, T. R.; Sigdel, K. P.; Utjesanovic, M.; Marsh, B. P.; Gallazzi, F.; Smith, V. F.; Kosztin, I.; King, G. M. Single-Molecule PeptideLipid Affinity Assay Reveals Interplay between Solution Structure and Partitioning. *Langmuir* **2017**, *33*, 4057−4065.

(21) Utjesanovic, M.; Matin, T. R.; Sigdel, K. P.; King, G. M.; Kosztin, I. Multiple Stochastic Pathways in Forced Peptide-Lipid Membrane Detachment. *Sci. Rep.* **2019**, *9*, 451.

(22) Marshall, B. T.; Long, M.; Piper, J. W.; Yago, T.; McEver, R. P.; Zhu, C. Direct Observation of Catch Bonds Involving Cell-Adhesion Molecules. *Nature* **2003**, *423*, 190−193.

(23) Churnside, A. B.; Sullan, R. M.; Nguyen, D. M.; Case, S. O.; Bull, M. S.; King, G. M.; Perkins, T. T. Routine and timely sub-picoNewton force stability and precision for biological applications of atomic force microscopy. *Nano Lett.* **2012**, *12*, 3557−61.

(24) Zimmermann, J. L.; Nicolaus, T.; Neuert, G.; Blank, K. Thiol-based, site-specific and covalent immobilization of biomolecules for single-molecule experiments. *Nat. Protoc.* **2010**, *5*, 975−85.

(25) Tamm, L. K.; McConnell, H. M. Supported phospholipid bilayers. *Biophys. J.* **1985**, *47*, 105−113.

(26) Cremer, P.; Boxer, S. Formation and Spreading of Lipid Bilayers on Planar Glass Supports. *J. Phys. Chem. B* **1999**, *103*, 2554.

(27) MacCallum, J. L.; Bennett, W. F. D.; Tieleman, D. P. Distribution of Amino Acids in a Lipid Bilayer from Computer Simulations. *Biophys. J.* **2008**, *94*, 3393−3404.

(28) Pogorelov, T. V.; Vermaas, J. V.; Arcario, M. J.; Tajkhorshid, E. Partitioning of Amino Acids into a Model Membrane: Capturing the Interface. *J. Phys. Chem. B* **2014**, *118*, 1481−1492.

(29) Holzwarth, G.; Doty, P. The Ultraviolet Circular Dichroism of Polypeptides1. *J. Am. Chem. Soc.* **1965**, *87*, 218−228.

(30) Greenfield, N. J.; Fasman, G. D. Computed circular dichroism spectra for the evaluation of protein conformation. *Biochemistry* **1969**, *8*, 4108−4116.

(31) Venyaminov, S. Y.; Baikalov, I. A.; Shen, Z. M.; Wu, C. S. C.; Yang, J. T. Circular Dichroic Analysis of Denatured Proteins: Inclusion of Denatured Proteins in the Reference Set. *Anal. Biochem.* **1993**, *214*, 17−24.

(32) Holtzer, M. E.; Holtzer, A. α-helix to random coil transitions: Determination of peptide concentration from the CD at the isodichroic point. *Biopolymers* **1992**, *32*, 1675−1677.
(33) Evans, E.; Leung, A.; Heinrich, V.; Zhu, C. Mechanical Switching and Coupling between Two Dissociation Pathways in a P-Selectin Adhesion Bond. *Proc. Natl. Acad. Sci. U. S. A.* **2004**, *101*, 11281−11286.
(34) Pereverzev, Y. V.; Prezhdo, O. V.; Forero, M.; Sokurenko, E. V.; Thomas, W. E. The Two-Pathway Model for the Catch-Slip Transition in Biological Adhesion. *Biophys. J.* **2005**, *89*, 1446−1454.
(35) Humphrey, W.; Dalke, A.; Schulten, K. VMD: visual molecular dynamics. *J. Mol. Graphics* **1996**, *14* (33−38), 27−28.
(36) Kabsch, W.; Sander, C. Dictionary of protein secondary structure: Pattern recognition of hydrogen-bonded and geometrical features. *Biopolymers* **1983**, *22*, 2577−2637.
(37) Findik, B. T.; Smith, V. F.; Randall, L. L. Penetration into membrane of amino-terminal region of SecA when associated with SecYEG in active complexes: Penetration of SecA N Terminus into a Membrane Bilayer. *Protein Sci.* **2018**, *27*, 681−691.
(38) Allen, W. J.; Corey, R. A.; Oatley, P.; Sessions, R. B.; Baldwin, S. A.; Radford, S. E.; Tuma, R.; Collinson, I. Two-way communication between SecY and SecA suggests a Brownian ratchet mechanism for protein translocation. *eLife* **2016**, *5*, No. e15598.
(39) Bariya, P.; Randall, L. L. Coassembly of SecYEG and SecA Fully Restores the Properties of the Native Translocon. *J. Bacteriol.* **2019**, *201*, e00493−18.
(40) Oliver, D. Substrate Proteins Take Shape at an Improved Bacterial Translocon. *J. Bacteriol.* **2019**, *201*, e00618−18.
(41) Sanganna Gari, R. R.; Chattrakun, K.; Marsh, B. P.; Mao, C.; Chada, N.; Randall, L. L.; King, G. M. Direct visualization of the *E. coli* Sec translocase engaging precursor proteins in lipid bilayers. *Science Advances*, in press **2019**, *5*eaav9404
(42) Kramer, G.; Boehringer, D.; Ban, N.; Bukau, B. The ribosome as a platform for co-translational processing, folding and targeting of newly synthesized proteins. *Nat. Struct. Mol. Biol.* **2009**, *16*, 589−597.
(43) Tomkiewicz, D.; Nouwen, N.; van Leeuwen, R.; Tans, S.; Driessen, A. J. M. SecA Supports a Constant Rate of Preprotein Translocation. *J. Biol. Chem.* **2006**, *281*, 15709−15713.
(44) Liang, F.-C.; Bageshwar, U. K.; Musser, S. M. Bacterial Sec Protein Transport Is Rate-limited by Precursor Length: A Single Turnover Study. *Mol. Biol. Cell* **2009**, *20*, 4256−4266.
(45) Fessl, T.; Watkins, D.; Oatley, P.; Allen, W. J.; Corey, R. A.; Horne, J.; Baldwin, S. A.; Radford, S. E.; Collinson, I.; Tuma, R. Dynamic action of the Sec machinery during initiation, protein translocation and termination. *eLife* **2018**, *7*, No. e35112.
(46) van der Wolk, J. P. W.; de Wit, J. G.; Driessen, A. J. M. The catalytic cycle of the Escherichia coli SecA ATPase comprises two distinct preprotein translocation events. *EMBO Journal* **1997**, *16*, 7297−7304.
(47) Breukink, E.; Nouwen, N.; van Raalte, A.; Mizushima, S.; Tommassen, J.; de Kruijff, B. The C Terminus of SecA Is Involved in Both Lipid Binding and SecB Binding. *J. Biol. Chem.* **1995**, *270*, 7902−7907.
(48) Sigdel, K.; Pittman, A.; Matin, T.; King, G. In High-Resolution AFM-Based Force Spectroscopy; Lyubchenko, Y. L., Ed.; *Nanoscale Imaging. Methods in Molecular Biology*; Humana Press: New York, 2018; Vol. *1814*.
(49) Andrecka, J.; Spillane, K. M.; Ortega-Arroyo, J.; Kukura, P. Direct Observation and Control of Supported Lipid Bilayer Formation with Interferometric Scattering Microscopy. *ACS Nano* **2013**, *7*, 10662−10670.
(50) Chada, N.; Sigdel, K.; Sanganna Gari, R.; Matin, T.; Randall, L.; King, G. Glass is a Viable Substrate for Precision Force Microscopy of Membrane Proteins. *Sci. Rep.* **2015**, *5*, 12550.
(51) Wu, E. L.; Cheng, X.; Jo, S.; Rui, H.; Song, K. C.; Dvila-Contreras, E. M.; Qi, Y.; Lee, J.; Monje-Galvan, V.; Venable, R. M.; Klauda, J. B.; Im, W. CHARMM-GUI *Membrane* Builder toward realistic biological membrane simulations. *J. Comput. Chem.* **2014**, *35*, 1997−2004.
(52) Lee, J.; Cheng, X.; Swails, J. M.; Yeom, M. S.; Eastman, P. K.; Lemkul, J. A.; Wei, S.; Buckner, J.; Jeong, J. C.; Qi, Y.; et al. CHARMM-GUI Input Generator for NAMD, GROMACS, AMBER, OpenMM, and CHARMM/OpenMM Simulations Using the CHARMM36 Additive Force Field. *J. Chem. Theory Comput.* **2016**, *12*, 405−413.
(53) Phillips, J. C.; Braun, R.; Wang, W.; Gumbart, J.; Tajkhorshid, E.; Villa, E.; Chipot, C.; Skeel, R. D.; Kal, L.; Schulten, K. Scalable molecular dynamics with NAMD. *J. Comput. Chem.* **2005**, *26*, 1781−1802.
(54) Brooks, B. R.; Brooks, C. L.; Mackerell, A. D.; Nilsson, L.; Petrella, R. J.; Roux, B.; Won, Y.; Archontis, G.; Bartels, C.; Boresch, S.; et al. CHARMM: The biomolecular simulation program. *J. Comput. Chem.* **2009**, *30*, 1545−1614.
(55) Klauda, J. B.; Venable, R. M.; Freites, J. A.; O'Connor, J. W.; Tobias, D. J.; Mondragon-Ramirez, C.; Vorobyov, I.; MacKerell, A. D.; Pastor, R. W. Update of the CHARMM All-Atom Additive Force Field for Lipids: Validation on Six Lipid Types. *J. Phys. Chem. B* **2010**, *114*, 7830−7843.
(56) Gowers, R. J.; Linke, M.; Barnoud, J.; Reddy, T. J.; Melo, M. N.; Seyler, S. L.; Dotson, D. L.; Domanski, J.; Buchoux, S.; Kenney, I. M. MDAnalysis: a Python package for the rapid analysis of molecular dynamics simulations. *Proceedings of the 15th Python in Science Conference*. 2016; pp 98−105.
(57) Michaud-Agrawal, N.; Denning, E. J.; Woolf, T. B.; Beckstein, O. MDAnalysis: A toolkit for the analysis of molecular dynamics simulations. *J. Comput. Chem.* **2011**, *32*, 2319−2327.
(58) McGibbon, R. T.; Beauchamp, K. A.; Harrigan, M. P.; Klein, C.; Swails, J. M.; Hernández, C. X.; Schwantes, C. R.; Wang, L.-P.; Lane, T. J.; Pande, V. S. MDTraj: A Modern Open Library for the Analysis of Molecular Dynamics Trajectories. *Biophys. J.* **2015**, *109*, 1528−1532.
(59) Kelly, S. M.; Price, N. C. The use of circular dichroism in the investigation of protein structure and functions. *Curr. Protein Pept. Sci.* **2000**, *1*, 349−384.
(60) Wei, Y.; Thyparambil, A. A.; Latour, R. A. Protein Helical Structure Determination Using CD Spectroscopy for Solutions with Strong Background Absorbance from 190−230 nm. *Biochim. Biophys. Acta, Proteins Proteomics* **2014**, *1844*, 2331−2337.
(61) Duarte, A. M.S.; Wolfs, C. J.A.M.; van Nuland, N. A.J.; Harrison, M. A.; Findlay, J. B.C.; van Mierlo, C. P.M.; Hemminga, M. A. Structure and localization of an essential transmembrane segment of the proton translocation channel of yeast H^+-V-ATPase. *Biochim. Biophys. Acta, Biomembr.* **2007**, *1768*, 218−227.
(62) Dudko, O. K.; Hummer, G.; Szabo, A. Intrinsic Rates and Activation Free Energies from Single-Molecule Pulling Experiments. *Phys. Rev. Lett.* **2006**, *96*, 108101−4.
(63) Dudko, O. K.; Hummer, G.; Szabo, A. Theory, Analysis, and Interpretation of Single-Molecule Force Spectroscopy Experiments. *Proc. Natl. Acad. Sci. U. S. A.* **2008**, *105*, 15755−15760.
(64) Bell, G. I. Models for the Specific Adhesion of Cells to Cells. *Science* **1978**, *200*, 618−627.
(65) Evans, E.; Ritchie, K. Dynamic Strength of Molecular Adhesion Bonds. *Biophys. J.* **1997**, *72*, 1541−1555.
(66) Hummer, G.; Szabo, A. Kinetics from Nonequilibrium Single-Molecule Pulling Experiments. *Biophys. J.* **2003**, *85*, 5−15.
(67) Risken, H. *The Fokker-Planck Equation: Methods of Solution and Applications*, 3rd ed.; Springer-Verlag Telos: 1996.

https://dx.doi.org/10.1021/acs.langmuir.9b03606
Langmuir 2020, 36, 2143−2152